Mechatronics and Automation Technology
J. Xu (Ed.)

doi:10.3233/ATDE221179

Localization of Wall Climbing Robot on Cylinder-Shaped Steel

Wen ZHANG, Tianzhi HUANG and Zhenguo SUN[1]
Department of Mechanical Engineering, Tsinghua University, Beijing, China.

Abstract. Due to the limitation of sensor application in special environment such as relatively closed and magnetic interference environment, the positioning and the heading angle errors of wall climbing robots accumulate with time. This paper proposes a difference projection localization method based on an external RGB-D camera and a robot-carried inertial measurement unit (IMU). We differential the depth image to obtain the distance change due to the robot occupancy. Then, the 3D point cloud information is converted into 2D image information by projecting the above distances along the normal vector of the robot chassis, which greatly speeds up the computational speed. The position of the robot is calculated by studying the statistical characteristics of the projection. Two EKFs are designed to estimate the attitude, taking the gravity vector and the normal vector of the robot chassis as observation. The experimental results show that the localization error of the wall climbing robot is within 0.017m, and the heading angle error of the attitude estimation is within 3.1°. The obtained results prove its applicability in self-localization of the wall climbing robot.

Keywords. Sensor fusion, extended Kalman filter, wall climbing robot.

1. Introduction

With the development of robot technology, the magnetic adsorption wall climbing robot [1] replaces people to carry out high-altitude work on the surface of large components, which improves the work efficiency, saves the cost of building scaffolds, and eliminates the danger of manual work. Localization is the basis for the wall climbing robot to achieve autonomous navigation. After positioning, path planning is carried out to enable the wall climbing robot to automatically climb on the surface of vertical large components and perform cleaning, flaw detection, repair welding and other operations. At present, the sensors used in robot positioning include cameras, light detection and ranging (LIDAR), wireless positioning sensors and information fusion of various sensors.

Large steel components such as storage tanks and turbine blades have smooth surfaces, and neither 2D nor 3D LIDAR can realize positioning function due to lack of effective edge information [2]. In order to prevent rust, the surfaces of large components are generally uniformly sprayed. The visual SLAM methods of robot-carried cameras, such as ORB-SLAM3 [3], PL-SLAM [4], SVO2 [5], are easy to lose features in the process of motion tracking. Wireless positioning methods such as WiFi [6], radio frequency identification (RFID) [7-8] and ultra wide band (UWB) [9] methods are

[1] Corresponding Author, Zhenguo SUN, Department of Mechanical Engineering, Tsinghua University, Beijing, China; E-mail: sunzhg@tsinghua.edu.cn.

widely used in indoor, tunnel, factory et al., but the multi-path reflection caused by the absorption and occlusion of steel components to signals affects the positioning accuracy.

The inertial navigation method based on IMU sensors is not affected by the working environment of the wall climbing robot, but the position and heading angle errors caused by the drift of IMU need to be corrected by external information. Since the wall climbing robot usually adopts the magnetic adsorption method, it is limited to correct the heading angle through the magnetometer.

In order to solve the above problems, this paper uses external cameras to assist the IMU to estimate the position and attitude of the wall climbing robot. Zhang Y [10] localized the robot using the an ArUco marker attached on the robot through the external surveillance camera. Yasuda S et al. [11] installed build-in LEDs on the top board of the robot, and used a stereo camera to locate the mobile robots by detecting the bright part of the optical images. However, the above methods need to change the original structure of the robot, and these marks are easily shielded by the dust in the working environment of the industrial robot. Partanen T [12] proposed a widely deployable scheme of fixed camera-based object positioning utilizing the CNN-detector. The middle point of the bottom boundary of extracted bounding box was used as the object root point. However, the positioning accuracy needs to be further improved and no attitude information is provided.

This paper proposes a differential projection method to fuse the information of RGB-D camera and IMU, convert the 3D point cloud information of the robot into 2D single channel image information, and improve the speed of positioning. The position of the robot is directly obtained by the RGB-D camera, and the heading angle is corrected by the normal vector at the contact point between the large component and the robot.

2. The Difference Projection Localization Method

The localization system in this paper is shown in figure 1. To represent the position and the attitude of wall climbing robots, the navigation coordinate system {n}, the IMU coordinate system {i}, the body coordinate system {b}, and the camera coordinate system {R} are defined. The flow chart of the proposed method in this paper is shown in figure 2. We will introduce the principle of the differential projection method in Section 2.1, describe the position estimation in Section 2.2, and present the attitude estimation in detail in Section 2.3.

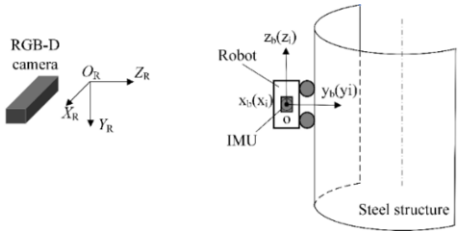

Figure 1. Localization of the wall climbing robot

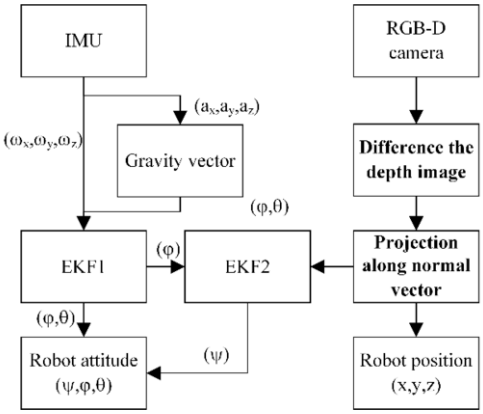

Figure 2. The flow chart of the difference projection localization method

2.1. Principle of the Difference Projection Method

Only the area of the wall-climbing robot in the field of vision is changed during the localization. To speed up the algorithm, we process only the area occupied by the robot and obtain the rough position by differencing the depth image. Before placing the robot, the RGB image (shown in figure 3a) and the depth image of the large component are acquired, and a 3D point cloud of the large component is calculated based on the pinhole camera model. The above operation that is performed only once during the initialization. Let the distance at (u, v) in the depth image corresponding to figure 3a be $d_0(u,v)$. During movement of the robot, an RGB image is obtained as shown in figure 3b. Let the distance at (u, v) in the depth image corresponding to figure 3b be $d(u,v)$.The depth image of the robot occupied area obtained by equation (1) is shown in figure 3c. The local area of the large component is approximated as a plane. After obtaining the rough position of the robot, the normal vector at the contact between the robot and the large component is estimated from the 3D point cloud of the large component, which is collineation with the normal vector of the robot chassis.

$$\Delta d(u,v) = d(u,v) - d_0(u,v) \tag{1}$$

Only a rough estimate of position can be obtained after difference. The method of setting color markers on the robot shell as reference points is susceptible to interference from illumination and similar color areas in the environment. To solve these problems, a location method based on normal vector projection is proposed. The projection schematic is shown in figure 4. RGB-D camera obtains the distance of each pixel through time of flight (TOF). Because of the occupation of the robot, the point P_t on the top of the robot moves to P_{t0}, and the point P_a around the robot moves to P_{a0}. The distances of line L_t and L_a are reduced by $|P_tP_{t0}|$ and $|P_aP_{a0}|$ respectively in the direction of light path. Therefore, the pixels on the top and side of the robot shell can be distinguished according to the distance change in the direction of the light path.

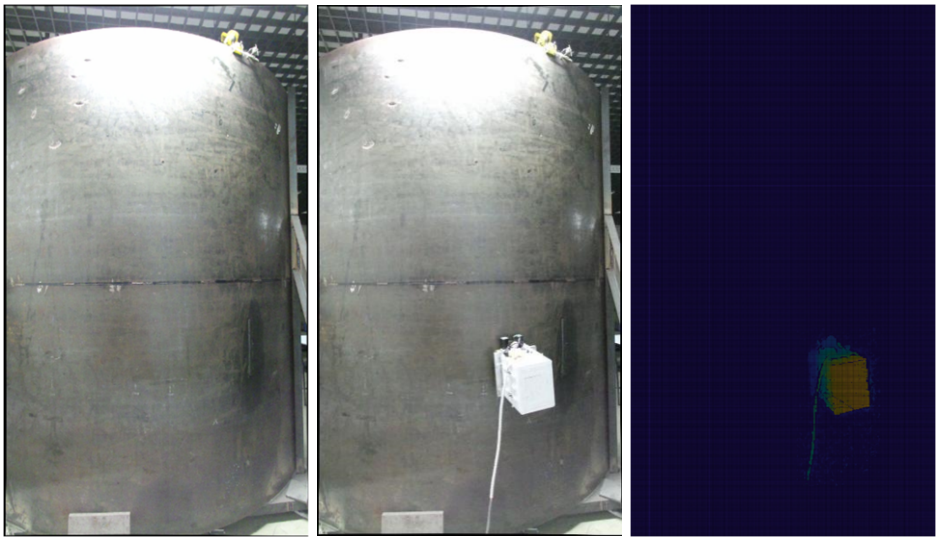

(a) (b) (c)

Figure 3. The initial position of the robot is obtained by the difference of the depth image (a) The large steel component. (b) The robot is moving on the large steel component. (c) Depth image after difference.

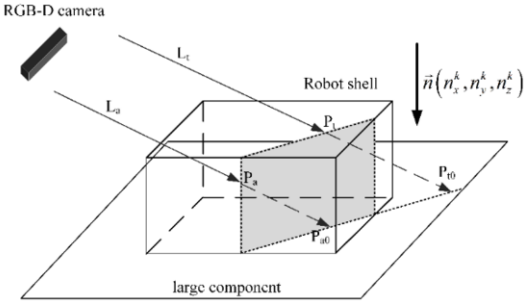

Figure 4. Projection of robot point cloud in the direction of normal vector. Position change of point cloud is caused by robot occupancy.

2.2. Position Estimation

According to the pinhole camera model, the point cloud displacement (in figure 4) due to robot occupancy is as follows,

$$\overrightarrow{P_tP_{t0}}=\overrightarrow{OP_t}-\overrightarrow{OP_{t0}}=\left(\frac{u-c_x}{f_x},\frac{v-c_y}{f_y},1\right)\frac{1}{s}\Delta d(u,v) \tag{2}$$

The inclined line segment corresponding to the top of the robot is the longest, while the side edge of the robot is shorter. Let $\vec{n}\left(n_x^k,n_y^k,n_z^k\right)$ be the normal vector of the robot chassis, which is collinear with the normal vector at the contact area of the robot and the

large component. The inclined line segment $\overrightarrow{P_t P_{t0}}$ is projected along the $\vec{n}$ in equation (3). The projected length $h(u,v)$ of the inclined line corresponding to the top of the robot is approximately equal to the robot height *H*, while the side is less than *H*. Through equation (3), we convert 3D information into 2D single channel image information.

$$h(u,v) = \overrightarrow{P_t P_{t0}} \cdot \vec{n} \tag{3}$$

In the 3D point set $\{k_{u,v} | h(u,v) = H\}$ of the robot top, we select $M(M_x, M_y, M_z)$ as the position of the robot.

$$(M_x, M_y, M_z)^{\mathrm{T}} = \frac{1}{N}\sum_{1}^{N} k_{u,v} \tag{4}$$

2.3. Attitude Estimation

After the wall climbing robot reaches the destination through location, it also needs to realize the adjustment of the end operation unit. An attitude estimation method based on two EKFs is adopted to realize the orientation of the wall climbing robot.

The Euler Angle representation of robot attitude, such as roll angle ϕ, pitch angle θ and heading angle ψ is introduced. The Euler Angle is defined in the following order: the first rotation of -ψ about the axis Z, the second rotation of θ about the new axis Y, and the third rotation of ϕ about the latest axis X. The direction cosine matrix corresponding to the order of the defined Euler Angle is shown in equation (5), which represents the rotation matrix from the robot body coordinate system to the navigation coordinate system.

$$ {}^{n}_{b}C = \begin{bmatrix} \theta_c\psi_c & -\phi_c\psi_s + \phi_s\theta_s\psi_c & \phi_s\psi_s + \phi_c\theta_s\psi_c \\ \theta_c\psi_s & \phi_c\psi_c + \phi_s\theta_s\psi_s & -\phi_s\psi_c + \phi_c\theta_s\psi_s \\ -\theta_s & \phi_s\theta_c & \phi_c\theta_c \end{bmatrix} \tag{5}$$

here, the lower subscript "*s*" represents the corresponding sine function value, and "*c*" represents the corresponding cosine function value.

2.3.1 The First EKF

The first EKF is designed to calculate the pitch and roll angles of the wall climbing robot, taking the direction of gravity as a reference. The state ${}^{1}\boldsymbol{x}_k$ consists of the third row elements in ${}^{n}_{b}\boldsymbol{C}$ and the angular velocity drift of the IMU,

$${}^{1}\boldsymbol{x}_k = \left(C_{31}^k\ C_{32}^k\ C_{33}^k\ b_x^k\ b_y^k\ b_z^k\right)^{\mathrm{T}} \tag{6}$$

According to directional cosine method [13], write the recursive relation of state ${}^1\boldsymbol{x}_k$ as follows,

$$ {}^1x_{k+1} = f\left({}^1x_k\right) = {}^1x_k + t_\mathrm{s}\begin{pmatrix}\left[C_{3\times}\right]_k \\ 0_{3\times3}\end{pmatrix}\begin{pmatrix}\omega_x^k - b_x^k \\ \omega_y^k - b_y^k \\ \omega_z^k - b_z^k\end{pmatrix} + \begin{pmatrix}\boldsymbol{W}_\mathrm{c}^k \\ \boldsymbol{W}_\mathrm{b}^k\end{pmatrix} \tag{7} $$

Here, $\boldsymbol{W}_b^k$ and $\boldsymbol{W}_c^k$ are zero mean process white noise vectors.

$$ \left[C_{3\times}\right]_k = \begin{pmatrix}0 & -C_{33}^k & C_{32}^k \\ C_{33}^k & 0 & -C_{31}^k \\ -C_{32}^k & C_{31}^k & 0\end{pmatrix} \tag{8} $$

The system state transition matrix ${}^1\boldsymbol{F}_k$ is shown in equation (9),

$$ {}^1\boldsymbol{F}_k = \frac{\partial f\left({}^1\boldsymbol{x}_k\right)}{\partial\left({}^1\boldsymbol{x}_k\right)} \tag{9} $$

The wall-climbing robot moves at a low speed on the surface of large components with an acceleration close to zero. The output of accelerometer in IMU is approximately equal to gravity, which could be selected as the observation ${}^1\boldsymbol{z}_k$. The observation equation of the first EKF is shown as equation (10),

$$ {}^1\boldsymbol{z}_k = \left(a_x^k\ a_y^k\ a_z^k\right)^\mathrm{T} = \boldsymbol{H}_1\,{}^1\boldsymbol{x}_k + {}^1\boldsymbol{v}_k \tag{10} $$

$$ \boldsymbol{H}_1 = \left(-g\boldsymbol{I}_3 \quad \boldsymbol{0}_{3\times3}\right) \tag{11} $$

Here, $\boldsymbol{H}_1$ is the observation matrix, and ${}^1\boldsymbol{v}_k$ is the observation noise vector.

Autocorrelation matrix ${}^1\boldsymbol{Q}_k$ of state noise and Covariance matrix ${}^1\boldsymbol{R}_k$ of observation noise are shown in equation (12) and (13) respectively,

$$ {}^1\boldsymbol{Q}_k = t_\mathrm{s}^2\begin{pmatrix}\sigma_\mathrm{c}^2\boldsymbol{I}_3 & 0_{3\times3} \\ 0_{3\times3} & \sigma_\mathrm{b}^2\boldsymbol{I}_3\end{pmatrix} \tag{12} $$

$$ {}^1\boldsymbol{R}_k = \left(\hat{a}_k\sigma_\mathrm{a}^2 + \sigma_\mathrm{f}^2\right)\boldsymbol{I}_3 \tag{13} $$

Where σ_c^2 is the estimate variance of the third row elements in ${}_b^n\boldsymbol{C}$, and σ_b^2 is the estimate variance of angular velocity drift. $\hat{a}_k$ is the estimated acceleration of the

robot. σ_{f}^2 is the measurement noise variance of acceleration. σ_{a}^2 is the variance of the estimated acceleration.

The iterative calculation steps of the first EKF can be found in the literature [13].

2.3.2 The Second EKF

The second EKF is designed to correct the robot's heading angle using the normal vector of the robot chassis as the observation. The state ${}^2x_k$ consists of the cosine and sine values of the heading angle, as shown in equation (14).

$$ {}^2x_k = \left(\cos\psi_k \ \sin\psi_k\right)^{\mathrm{T}} \tag{14}$$

Through the first EKF, the roll angle ϕ_k, the pitch angle θ_k and θ_{k+1} are obtained. The first two elements in the first column of ${}_b^n\boldsymbol{C}$ are iteratively calculated. As shown in Equation (15), the state equation of the second EKF can be obtained by multiplying both sides of the equation by $\left(\cos\theta_{k+1}\right)^{-1}$. The system state transition matrix is ${}^2F_k$,

$$ {}^2x_{k+1} = {}^2F_k \cdot {}^2x_k + \boldsymbol{W}_\psi^k \tag{15}$$

$$ {}^2F_k = \frac{1}{(\theta_c)_{k+1}} \begin{bmatrix} (\theta_c)_k + t_s\tilde{\omega}_z^k(\phi_s)_k(\theta_s)_k - t_s\tilde{\omega}_y^k(\phi_c)_k(\theta_s)_k & -t_s\tilde{\omega}_z^k(\phi_c)_k - t_s\tilde{\omega}_y^k(\phi_s)_k \\ t_s\tilde{\omega}_z^k(\phi_c)_k + t_s\tilde{\omega}_y^k(\phi_s)_k & (\theta_c)_k + t_s\tilde{\omega}_z^k(\phi_s)_k(\theta_s)_k - t_s\tilde{\omega}_y^k(\phi_c)_k(\theta_s)_k \end{bmatrix} \tag{16}$$

$$ \begin{cases} \tilde{\omega}_y^k = \omega_y^k - b_y^k \\ \tilde{\omega}_z^k = \omega_z^k - b_z^k \end{cases} \tag{17}$$

Where t_s is the sampling time of IMU, ω_y^k and ω_z^k are respectively the angular velocities of Y-axis and Z-axis at time *k*. b_y^k and b_z^k are respectively the angular velocity drifts of Y-axis and Z-axis in IMU at time *k*. $\boldsymbol{W}_\psi^k$ is the process white noise vector of zero mean.

Due to the interference of strong magnetic field, the magnetometer cannot be used to calibrate the heading angle of the wall climbing robot. The unit normal vector $\vec{n}\left(n_x^k, n_y^k, n_z^k\right)$ of the robot chassis is calculated through the 3D point cloud of large components obtained in Section 2.1. The new vector $(0\ 1\ 0)^{\mathrm{T}}$ obtained by projecting the vector $\vec{n}\left(n_x^k, n_y^k, n_z^k\right)$ in the navigation coordinate system to the robot body coordinate system through the attitude matrix ${}_b^nC^{\mathrm{T}}$ is also parallel to the y_{b} axis,

$$ \left(0\,1\,0\right)^{\mathrm{T}} = {}_b^nC^{\mathrm{T}} \cdot \left(n_x^k \ n_y^k \ n_z^k\right)^{\mathrm{T}} \tag{18}$$

Substituting equation (5) into equation (18), and eliminating θ_k:

$$\cos\phi_k = n_y^k \cos\psi_k - n_x^k \sin\psi_k \tag{19}$$

According to equation (19), the observation equation of the second EKF system is shown in equation (20). The cosine of roll angle is taken as the observation of the system, ${}^2\boldsymbol{z}_k = \cos\phi_k$,

$${}^2\boldsymbol{z}_k = H_2\,{}^2x_k + {}^2v_k \tag{20}$$

Here, the observation matrix $H_2 = \begin{pmatrix} n_y^k & -n_x^k \end{pmatrix}$, ${}^2v_k$ is the observation noise.

State noise autocorrelation matrix ${}^2\boldsymbol{Q}_k$ and covariance matrix ${}^2\boldsymbol{R}_k$ are shown in Equations (21) and (22):

$${}^2\boldsymbol{Q}_k = t_s^2 \begin{pmatrix} \sigma_{\psi 1}^2 & 0 \\ 0 & \sigma_{\psi 2}^2 \end{pmatrix} \tag{21}$$

$${}^2\boldsymbol{R}_k = \sigma_\phi^2 \tag{22}$$

Where $\sigma_{\psi 1}^2$ and $\sigma_{\psi 2}^2$ are the estimated variances of $\cos\psi_k$ and $\sin\psi_k$ respectively. σ_ϕ^2 is the measurement noise variance of $\cos\phi_k$.

The iterative calculation process of the second EKF is the same as the first EKF, replacing ${}^1x_k$, ${}^1F_k$, H_1 , ${}^1\boldsymbol{Q}_k$, ${}^1\boldsymbol{R}_k$ with ${}^2x_k$, ${}^2F_k$, H_2 , ${}^2\boldsymbol{Q}_k$, ${}^2\boldsymbol{R}_k$.

3. Experiments and discussion

To verify the effectiveness of the difference projection localization method, a wheeled permanent magnet adsorption wall climbing robot equipped with an IMU is used to conduct experiments on the surface of a large cylindrical steel component as shown in figure 5a. A Microsoft Kinect V2 camera (in figure 5b) with a resolution of 1920×1080 color image and 512×424 depth image is used to capture the images. The frequency of image acquisition is 8Hz. The ADIS16445 IMU (in figure 5c) is used to obtain angular velocity and acceleration. The sampling frequency of IMU is 100 Hz. It runs on Ubuntu 16.04 64-bit system, CPU: Intel i7 9750H, graphics card: GTX1050Ti, 16GB RAM. After initialization, the total running time of processing each frame does not exceed 100ms, and the algorithm we propose can achieve real-time location.

The color marking method based on binocular distance measurement are used to calculate the real position and attitude of the wall climbing robot. Three markers (red, blue and purple) with a diameter of 8mm are placed on the top of the robot, as shown in figure 5a. The 3-dimensional coordinate of the red marker are used as the real position of the wall climbing robot. Reference transformation matrix were computed through the Gram-Schmidt orthogonalization. The ZED binocular stereo camera is used to acquired images, and the measurement error of a single marker in the depth direction is calculated according to equation (23),

$$dz = \frac{z^2 \cdot de}{f \cdot b} \tag{23}$$

where z is the distance between the camera and the robot, z=1.2m; de is the parallax reading error, de=0.5pix; f is the focal length, f=1400pix; b is the baseline length, b=0.12m. According to equation (23), dz is not more than 4.3mm.

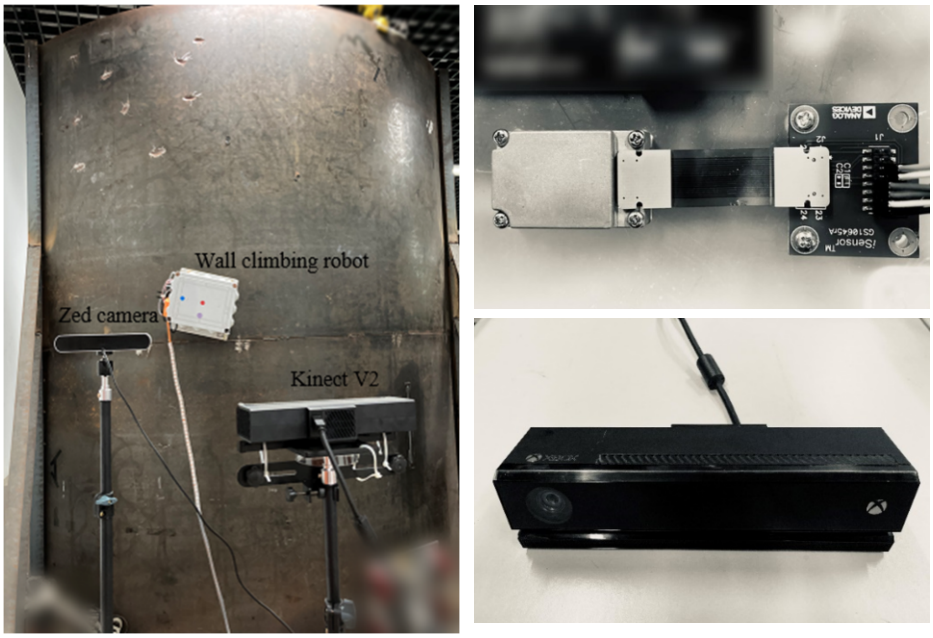

Figure 5. (a) Localization system of the wall climbing robot for experiments (b) ADIS16445 IMU (c) Kinect v2 RGB-D camera.

The design of the experiments is as follows: (1) Let the wall climbing robot move along the horizontal route (Path 1) on the surface of the large component through the ground remote control, as shown in figure 6a. (2) Let the robot move in the edge of camera field of vision along circular route (Path 2), as shown in figure 6b. (3) Let the robot move along the Path 3, as shown in figure 6c.

3.1. Position errors

The absolute trajectories of the wall climbing robot are illustrated in figure 6. The black line represents the ground truth, and the red line represents the trajectory estimated by our proposed method. The center of the target rectangular obtained by CNN-detector [12] is located to estimate the position directly, and the result is represented by blue line.

As shown in figure 6c, the trajectory calculated by our proposed method is consistent with the ground truth, when the wall climbing robot moves in the middle area of the camera's field of vision. Figure 7a and figure 7b correspond to Path 1 in figure 6a and Path 2 in figure 6b respectively. The maximum absolute trajectory error of our method is 0.017m, while the method of CNN method is 0.1m. The proposed method has

a much smaller deviation from the real value, concluded from the peaks in figure 7a and 7b.

Figure 7c corresponds to Path 3 in figure 6c. For both methods, the position accuracy of the robot in the center area of the camera's field of vision is superior to that in the edge area, revealed in figure 7c. For few peaks over 0.05m in figure 7c, the robot moves in the center of the camera's field of view most of the time. In our method, the projection for robot position is sensitive to the normal vector of the robot chassis, which is preliminarily estimated according to the difference of the depth image. A more accurate estimation of the robot chassis normal vector will help to improve the positioning accuracy of the robot in the edge area. Experiments results show that the difference projection localization method can effectively locate the wall-climbing robot, meeting the positioning requirements of industrial robot task and path planning.

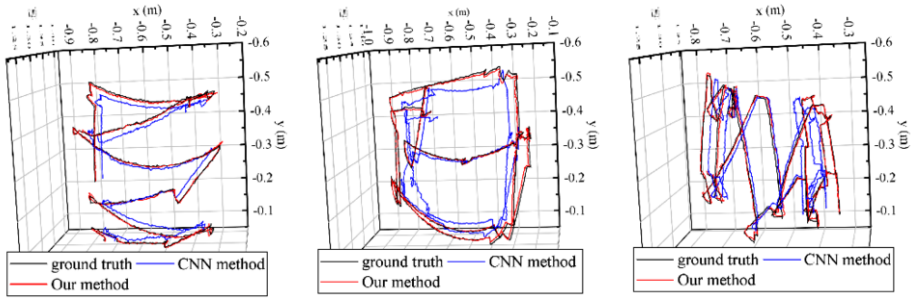

Figure 6. The absolute trajectories of CNN method compared with our method in different paths. (a) Path 1. (b) Path 2. (c) Path 3.

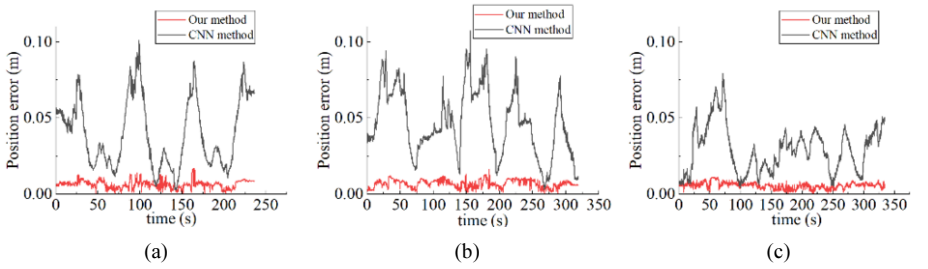

Figure 7. The absolute trajectory error of CNN method compared with our method in different paths. (a) Path 1. (b) Path 2. (c) Path 3.

3.2. Attitude Errors

Most of the existing external camera localization methods (including the CNN method in the literature [12]) that do not apply marker points do not provide a attitude estimation function, so we can only use the Madgwick method [14] to compare with the proposed method. Due to magnetic interference, the correction function of magnetometer for

heading angle cannot be used. The calculation of roll angle and pitch angle by the two methods are almost the same. We focus on the estimation results of heading angle. Figure 8a and figure 8b correspond to Path 1 in figure 6a and Path 2 in figure 6b respectively. The maximum pitch angle error is 1° and the maximum roll angle error is 2.4°. When the robot moves in the vertical line, there is no large rotation, and the roll angle and pitch angle are less affected by the motion acceleration, and the maximum error is less than 1°. The maximum heading angle error using Madgwick method is 6.7° and increases with time elapsing, while the maximum heading angle error of our method is less than 3.1°.

The observation of heading angle in the second EKF is the normal vector of robot chassis. When the robot moves in the left and right regions in figure 5a, the estimation of the robot chassis normal vector deviates from the correct value, as shown in figure 8a and figure 8b. When the robot moves in the center area of the camera's field of view, the maximum heading angle error shown in the blue line is less than 1°, as shown in 8c.

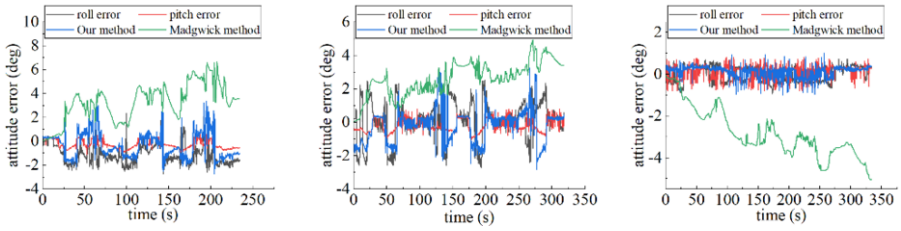

Figure 8. The attitude error of our method in different paths. (a) Path 1. (b) Path 2. (c) Path 3.

4. Conclusion

In this paper, we presented a difference projection localization method based on an external RGB-D camera and an IMU to solve the problem of accumulated positioning and heading angle errors in wall climbing robots. The rough position of the robot is obtained by the difference of the depth image. After that, the 3D point cloud information is converted into 2D image information by projecting along the direction of the normal vector of the robot chassis. Based on the height distribution of projection, we obtain the robot's position by statistics. Two EKFs are designed to reliably estimate the attitude, taking the gravity vector and the normal vector of the robot chassis as observation. The experimental results show that the localization error of the wall climbing robot is within 0.017m and the heading angle error of the attitude estimation is within 3.1° The pitch angle error is within 1°. The roll angle error is within 2.4°. For future work, we would like to develop a multi-camera collaboration model to enable localization of wall climbing robots over a larger area.

Acknowledgements

The work is supported by the National Natural Science Foundation of China (E51475259).

References

[1] Ding Y, Sun Z, Chen Q. Non-contacted permanent magnetic absorbed wall-climbing robot for ultrasonic weld inspection of spherical tank[C]//MATEC Web of Conferences. EDP Sciences, 2019, 269: 02013.

[2] Park C, Moghadam P, Williams J L, et al. Elasticity meets continuous-time: Map-centric dense 3D LiDAR SLAM[J]. IEEE Transactions on Robotics, 2021, 38(2): 978-997.

[3] Campos C, Elvira R, Rodríguez J J G, et al. Orb-slam3: An accurate open-source library for visual, visual–inertial, and multimap slam[J]. IEEE Transactions on Robotics, 2021, 37(6): 1874-1890.

[4] Pumarola A, Vakhitov A, Agudo A, et al. PL-SLAM: Real-time monocular visual SLAM with points and lines[C]//2017 IEEE international conference on robotics and automation (ICRA). IEEE, 2017: 4503-4508.

[5] Forster C, Zhang Z, Gassner M, et al. SVO: Semidirect visual odometry for monocular and multicamera systems[J]. IEEE Transactions on Robotics, 2016, 33(2): 249-265.

[6] Sun W, Xue M, Yu H, et al. Augmentation of fingerprints for indoor WiFi localization based on Gaussian process regression[J]. IEEE Transactions on Vehicular Technology, 2018, 67(11): 10896-10905.

[7] Gunatilake A, Galea M, Thiyagarajan K, et al. Using UHF-RFID signals for robot localization inside pipelines[C]//2021 IEEE 16th Conference on Industrial Electronics and Applications (ICIEA). IEEE, 2021: 1109-1114.

[8] Gunatilake A, Kodagoda S, Thiyagarajan K. A Novel UHF-RFID Dual Antenna Signals Combined With Gaussian Process and Particle Filter for In-Pipe Robot Localization[J]. IEEE Robotics and Automation Letters, 2022, 7(3): 6005-6011.

[9] Barbieri L, Brambilla M, Trabattoni A, et al. UWB localization in a smart factory: Augmentation methods and experimental assessment[J]. IEEE Transactions on Instrumentation and Measurement, 2021, 70: 1-18.

[10] Zhang Y, Shi J, Wang Q, et al. An Exploration of Moving Robot Localization Assisted with a Static Monocular Camera[C]//2021 7th IEEE International Conference on Network Intelligence and Digital Content (IC-NIDC). IEEE, 2021: 6-10.

[11] Yasuda S, Kumagai T, Yoshida H. Calibration-free Localization for Mobile Robots Using an External Stereo Camera[C]//2020 IEEE International Conference on Consumer Electronics (ICCE). IEEE, 2020: 1-6.

[12] Partanen T, Müller P, Collin J, et al. Implementation and Accuracy Evaluation of Fixed Camera-Based Object Positioning System Employing CNN-Detector[C]//2021 9th European Workshop on Visual Information Processing (EUVIP). IEEE, 2021: 1-6.

[13] Wang Y, Rajamani R. Direction cosine matrix estimation with an inertial measurement unit[J]. Mechanical Systems and Signal Processing, 2018, 109: 268-284.

[14] Madgwick S O H, Harrison A J L, Vaidyanathan R. Estimation of IMU and MARG orientation using a gradient descent algorithm[C]//2011 IEEE international conference on rehabilitation robotics. IEEE, 2011: 1-7.